Composites & nanocomposites

Effect of electrophoretic deposition of micro-quartz on the microstructural and mechanical properties of carbon fibers and their bond performance toward cement

Huanyu Li[1,2], Marco Liebscher[1,*] , Khoa Hoang Ly[3], Phong Vinh Ly[3], Thomas Köberle[1], Jian Yang[2], Qingyi Fan[1], Minghao Yu[3], Inez M. Weidinger[3], and Viktor Mechtcherine[1]

[1] *Institute of Construction Materials, Technische Universität Dresden, 01062 Dresden, Germany*

[2] *State Key Laboratory of Ocean Engineering, Shanghai Key Laboratory for Digital Maintenance of Buildings and Infrastructure, School of Naval Architecture, Ocean and Civil Engineering, Shanghai Jiao Tong University, Shanghai 200240, People's Republic of China*

[3] *Faculty of Chemistry and Food Chemistry and Center for Advancing Electronics Dresden (Cfaed), Technische Universität Dresden, 01062 Dresden, Germany*

ABSTRACT

An electrophoretic deposition (EPD) process of micro-quartz (MQ) powder is applied to carbon fibers (CFs) with the aim to enhance their interfacial bond to cementitious matrices and to investigate its influence on the microstructural and mechanical properties of the CFs itself. The electrophoretic mobility of the MQ particles with negative charge in aqueous media was confirmed by potential sweep experiments and zeta-potential measurements. High amounts of MQ were successfully deposited onto the fiber surface, as proven by scanning electron microscopy. Single-fiber tension tests and thermogravimetric analysis showed that EPD treatment had little impact on the tensile properties and thermal stability of the modified fibers. However, storing the CFs in cement pore solution impaired temperature stability of untreated and modified fibers. X-ray diffraction and Raman spectroscopy reveal specific changes of CF's microstructure upon EPD treatment and immersion in pore solution. Single-fiber pullout tests showed that the pullout resistance of MQ-modified CFs was enhanced, relative to untreated CFs. This augmentation can be explained by an enhanced interlocking mechanisms between CF and matrix due to the deposited quartz particles on the CF surface.

🖄 Springer

Introduction

Cement-based composites, often referred to as concrete or mortar, are clearly dominant materials in the field of urban construction due to their numerous beneficial properties, such as convenience, high compressive strength, and high durability [1, 2]. However, their low flexural/tensile strength, low fracture toughness, and proneness to cracking limit often their efficient use, options of structural design as well as the serviceability of built structures [2, 3]. Considering the brittle nature of cementitious materials, various fiber reinforcements such as steel fibers, polymeric fibers, or carbon fibers (CFs) are increasingly used to improve their crack control capability and toughness [2, 4, 5]. CF is a promising engineering material having a number of advantages including high tensile strength and modulus of elasticity, relatively good chemical stability, and low density [6, 7]. These properties make CF an ideal candidate as reinforcement in building materials.

However, the inert CF surfaces exhibit a weak interaction with cementitious matrices, causing an insufficient force transfer from the matrix to fibers and thereby limiting the broader application of carbon fiber-reinforced concrete (CFRC) [8]. To enhance the bond of individual carbon filaments within a rowing and the bond of CF rovings toward concrete, commonly a polymer impregnation is used to glue the individual filaments together, so that the high strength of every single CF can be utilized [8, 9]. However, the applied polymer coating material considerably softens or even completely decomposes at high temperatures, in particular in the case of fire [10], drastically lowing stress-transfer capacity at the fiber–cement paste interface. Hence, an alternative approach has been developed using a thermal-stable impregnation suspension based on mineral particles [11]. Challenges related to this approach are difficulties to infiltrate the densely packed CF bundle as well as the hydrophobic CF surface hindering an efficient bond between the fiber and water-based mineral suspensions [12]. To overcome these issues, much work has been done in tailoring the surface wettability as well as the surface polarities of CFs [7, 13].

Schneider et al. [11] used low-pressure microwave plasma techniques at various gas conditions to modify the CF rovings and showed a dramatic increase in the bond strength between CF yarns and concrete matrices. Based on this research, Li et al. [8] investigated different oxygen plasma parameters and recommended a short-time treatment or stronger modification parameter to be beneficial. However, plasma treatment is not able to functionalize the internal fiber core, while the introduced functional groups may vanish over time [12, 14]. Owing to the good electrical conductivity of CFs, electrochemical treatments were performed to modify the CF surfaces [15, 16]. Li et al. [2] coated the CFs with calcite layers using electrochemical anodization in cementitious pore solution and indicated an increase in the maximum pullout force of a single fiber from the cement-based matrix. Note, some decline in the fiber tensile strength was reported for strong treatment conditions too.

Electrophoretic deposition (EPD) enables a homogeneous coating of CF surfaces with various materials on different scales [17–19]. During the EPD process, the charged particles move in the electrolytes according to the applied electrical field [20]. Based on this principle, nano-silica (NS) particles could be successfully grafted onto the surfaces of CFs and a compact interface could be attained at the peripheral zone of the fiber [17]. Since the NS coating layers can form calcium silicate hydrate (C–S–H), an enhanced interfacial bonding between the modified CFs and cement matrix was observed. In the previous studies [12, 21], the influence of EPD treatment on the microstructural and mechanical properties of CFs has been extensively investigated; however, the impact of the physicochemical environment of cement matrix on the CFs before and after modification is not clear so far.

In contrast to the reactive amorphous silica material, e.g., nano-silica [22] and micro-silica [23], crystalline quartz is generally considered to be chemically inert at room temperature [24], which also means it is not pozzolanically active in cementitious materials. However, it was found that quartz fume is not totally inert at high pH conditions and at elevated temperatures [25–28]. Furthermore, Benezet and Benhassaine [29, 30] reported that quartz powder below a particle diameter of about 5 μm showed a pozzolanic reactivity. Kadri et al. [31] added quartz fillers to Portland cement and noticed slightly accelerated hydration, which was more obvious for smaller particle sizes. According to [32–34], quartz fillers can promote the generation of calcium silicate hydrate

(C–S–H) by offering more crystallization nucleus. Bentz *et al.* [35] stated that both quartz and limestone powders were capable of diminishing the initial setting times and facilitating cement early-age hydration. The quartz particles at the macro scale, *i.e.*, the quartz sand, have been applied for the bond enhancement between CF multifilaments and cement-based matrices [9, 36], whereas the use of micro-scaled quartz in this regard is very scarce [37]. Furthermore, quartz exhibited negative zeta potentials in an aqueous solution owing to deprotonation on its surface, thus, indicating electrophoretic mobility [38, 39]. Nonetheless, to the best of the authors' knowledge, CF surface modification with quartz powders via EPD has not been reported as yet.

Hence, in the work at hand, CF surfaces are coated with quartz particles using EPD and aiming to strengthen the interfacial interaction between hydrophobic CF surfaces and cement-based materials. The coating layers formed are characterized by electron microscopy analysis, X-ray diffraction, and thermogravimetric analysis. Furthermore, the mechanical performance of the CFs before and after being stored in cementitious pore solution is analyzed by single-fiber tension tests, and their bond behavior toward matrices was measured by single-fiber pullout tests.

Materials and methods

Commercially available PAN-based epoxy-sized SIGRAFIL®C T50-4.4/255-E100 carbon fibers were obtained from SGL Group, Wiesbaden, Germany. Their main physical data are given in Table 1.

Micro-quartz (MQ) was bought from Sigma-Aldrich, Chemie GmbH, Munich, Germany, having a density of 2.6 g/cm^3 and an angular morphology, see Fig. 1a. Particle size distribution was measured by a laser diffraction particle size analyzer (LS 13,320, Beckman Coulter, Inc., Fullerton, USA), indicating diameters from 0.35 to 5.0 µm, see Fig. 1b. The

aqueous dispersion containing 1 wt.% MQ particles was produced by using an ultrasonicator (Bandelin Sonopuls HD 2070, Bandelin Electronics, Berlin, Germany) for 5 min just before the EPD process.

Electrophoretic deposition

To provide the electrical field in the EPD process, a Voltcraft LPS 1305 DC power supply from Conrad Electronic AG, Wollerau, Switzerland, was employed. A CF multifilament and a graphite cylinder served as the anodic and cathodic electrodes, respectively. The applied voltage of 1 V and treatment duration of 15 min were chosen based on the previous research [12].

After the surface modification process, the samples were cleaned with running distilled water four times to eliminate the weakly bonded particles from fiber surfaces. Then, these specimens were hung under a constant climate (24 °C, 55% relative humidity) for the drying process for 24 h.

To deliver clear insights into the interface reactions between modified CFs and cementitious matrices, the EPD-treated samples were immersed in a cementitious pore solution, which was prepared based on the previous study [2] and simulated the real cement environment. After 28 days of immersion, the CFs were observed by means of SEM.

Experimental characterization

Environmental scanning electron microscopy (ESEM, Quanta 250 FEG, FEI, Netherlands) was used to identify the morphology of CF surfaces, and energy-dispersive X-ray analysis (EDX, Quantax 400, Bruker) was used for elemental mapping. X-ray diffraction (XRD) analysis was carried out with a 3003-TT instrument from Seifert, Ahrensburg, Germany, to characterize the crystalline structure. Thermogravimetric analysis (TGA, NETZSCH Gerätebau GmbH, Selb, Germany) was implemented using an oxygen gas stream with a flow of 60 ml/min and heating rate of 10 °C/min. Zeta-potential ζ and pH value of the

Table 1 Main properties of the CFs under investigation (as provided by the supplier)

Filament diameter [µm]	Fineness of yarn [tex]	Density [g/cm^3]	Tensile strength [GPa]	Tensile modulus [GPa]	Elongation at break [%]	Number of filaments —
7.0	3420	1.8	4.4	255	1.65	50,000

Figure 1 **a** Morphology and **b** diameter distribution of quartz particles.
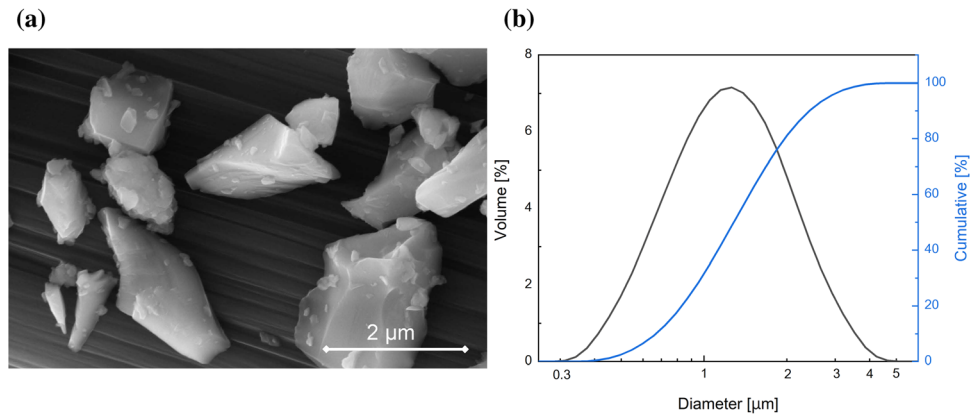
suspension were measured by a Field ESA analyzer from PA Partikel-Analytik-Messgeräte GmbH, Frechen, Germany, at ambient temperature. Potential sweep experiments were conducted by an electrochemical analyzer (CHI660E, USA) with a 9-mV s^{-1} scanning rate at the voltage in the range of -1 V to 1 V to assess the EPD process, during which the CF roving acted as the working electrode and a graphite rod as the counter electrode. The micromechanical tests including single-fiber tension tests and single-fiber pullout tests were carried out using a universal testing machine (Zwick Roell 1445, Ulm, Germany) with a 10-N load cell at a constant displacement rate of 0.01 mm/s, see Fig. 2.

For the fiber tensile strength measurements, the single filaments were individually fixed straightened onto a paper frame; the free length of fiber was 20 mm, see Fig. 2a. After mounting the samples, both vertical parts of the paper frames were removed prior to testing. Details of the setup can be found elsewhere [40]. At least 30 filaments were tested for each parameter under investigation.

In the fiber pullout experiments, the end of a single CF was embedded in a cementitious matrix with an embedded length of 1.2 mm to ensure the complete fiber pullout without fracture. The composition of the cement matrix was adopted from the previous research [41] and is given in Table 2. During pullout measurement, the free end of fibers was pulled at a constant speed of 0.01 mm/s. The setup configuration is illustrated in Fig. 2b, and its detailed description can also be found elsewhere [2]. For every parameter under investigation, seven or more samples were tested and then the obtained values were averaged.

Raman spectra were acquired with a confocal Raman microscope (S&I Monovista CRS +) equipped with a nitrogen-cooled detector (Pylon). As excitation, the 514 nm emission line of a Toptica Top mode single frequency 514 nm diode laser was used. The laser was focused on the sample using a 20 × objective (Nikon, NA 0.35) at a laser power of 2 mW. Spectra were calibrated with respect to mercury lines and the Raman spectrum of toluene. Spectra acquisition times ranged between 60 and 90 s, depending on the sample. Spectra treatment was performed using the in-house software Qpipsi based on the MATLAB (Wolfram Scientific).

Results and discussion

Zeta potential

The results of electrokinetic measurements are given in Table 3. Zeta-potential ζ of MQ suspension indicates a negative charge of the quartz particles. With -26.7 mV, it is in the range from ± 10 to ± 30 mV, demonstrating an incipient instability of this aqueous suspension based on ASTM Standard (D 4187-82) [42]. The negative charge of quartz particles was ascribed to the partial ionization of surficial silanol groups (–Si–OH), which provided hydrogen ions, resulting in a weak acidic pH value of MQ dispersion (pH = 6.57) [38, 39]. Thus, the charged MQ particles could move toward CF electrode surfaces with a counter-charge under the electrical field in the EPD system.

Figure 2 Setup for micromechanical tests: **a** single-fiber axial tension test and **b** one-sided single-fiber pullout test.
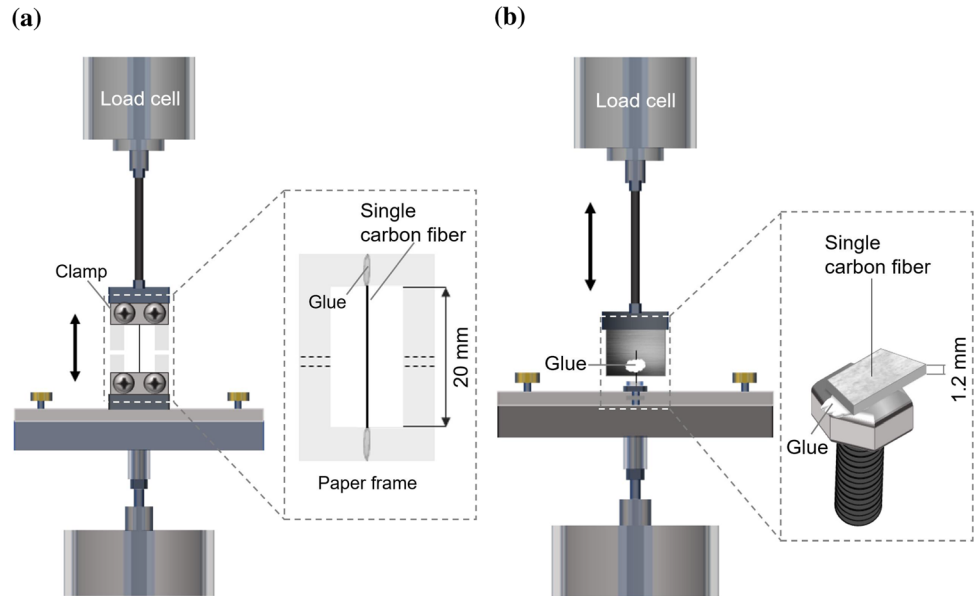
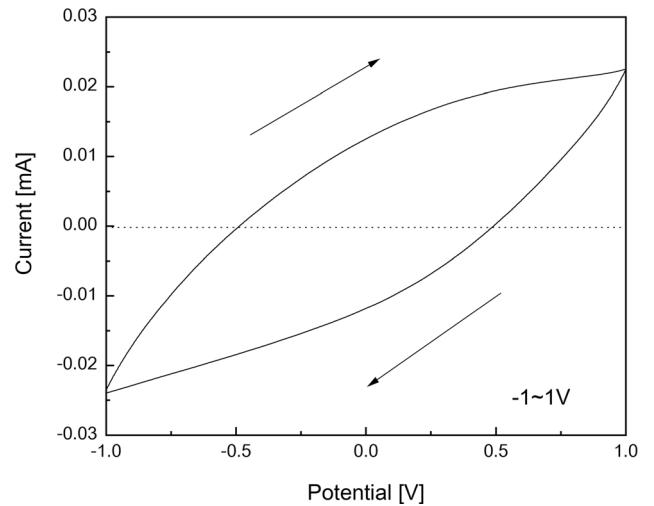**Table 2** Composition of the cementitious matrix for pullout experiments

Component	Content [kg/m^3]
Cement (CEM I 42.5 R) (Schwenk Zement KG, Germany)	505.0
Fly ash steament H4 (from black coal) (Herne, Germany)	621.0
Quartz sand (0.06–0.2 mm) (Strobel Quarzsand GmbH, Germany)	536.0
Viscosity Modifying Agent (Sika Deutschland GmbH)	4.8
Superplasticizer (MasterGlenium ACE 30) (BASF, Trostberg, Germany)	10.0
Water	338.0

Table 3 Zeta potential of 1 wt.% MQ particles in the dispersion

Measurement	pH [-]	Temperature [°C]	Zeta [mV]	Conductivity [mS/cm]
1	6.90	26.5	− 25.1	2023
2	6.67	26.5	− 23.7	2026
3	6.58	26.3	− 24.2	2020
4	6.57	26.2	− 25.8	2014
5	6.52	26.0	− 22.5	2010
6	6.51	25.8	− 29.9	2006
7	6.52	25.7	− 27.8	2010
8	6.55	25.6	− 27.5	2034
9	6.52	25.4	− 27.9	2060
10	6.51	25.3	− 29.4	2087
11	6.48	25.2	− 29.3	2094
Average	6.57	25.9	− 26.7	2035

Figure 3 Current response recorded for CF immersed into an aqueous MQ colloid solution upon potential sweeping with a rate of 9 mVs^{-1} from − 1 to + 1 V.

Potential sweep experiments

Figure 3 shows the recorded current response of MQ aqueous dispersion upon potential sweeping in the range from − 1 to + 1 V and vice versa. The current trace of the suspension displayed non-Ohmic response indicating the change of the electrode

resistances with potential. As previously discussed, this behavior can be rationalized by potential-induced adsorption and desorption of MQ particles, altering the surface charge of the electrode and hence the interface resistance [12]. In this model, MQ particles diffuse toward the positive electrode surfaces during the anodic scan from 0 to 1 V. Upon reverse sweeping from 1 to 0 V, electro-absorbed colloids onto CF yarn with a positive charge were partially detached. Sweeping from 0 to − 1 V leads to desorption of negatively charged particles from the CF electrode, which are reversibly deposited onto the counter electrode. The potential-induced surface adsorption process is fully reversible as indicated by the mirrored current responses.

Morphological analysis

Figure 4A presents the neat surfaces of pristine CFs with characteristic longitudinal grooves. After EPD treatment with MQ (1 V/15 min), a large number of quartz particles with various diameters were accumulated on the CF surfaces, see Fig. 4b. Notably, the particle size of these deposited quartz powders varied from the nanoscale to up to several micrometers, while no agglomeration of particles could be observed. Figure 5 shows an ESEM image and its

EDX elemental maps for the CF coated with MQ. The elements of Si and O confirmed the presence of MQ particles, indicating a successful deposition of quartz powder onto CF surfaces.

Figure 4c shows the appearance of as-received CFs after being stored in pore solution for 28 days. In comparison with the Ref sample, no obvious difference can be found except for some small mineral structures attached to fiber surfaces.

Figure 4d displays the surface morphology of MQ-modified CF (MQ-CF) after immersion into cement pore solution. Quartz particles remained on fiber surfaces after 28-d immersion. Interestingly, some mineral structures growing on the CFs' surfaces could be found, which potentially constitute calcite structures.

X-ray diffraction (XRD)

To better understand the crystalline structures of the modified CFs, X-ray diffraction (XRD) measurements were taken before and after exposure to cementitious pore solution. Figure 6 shows a major broad hump at around 25° for all the XRD curves, which is assigned to the graphitic (002) plane of CFs [43].

Figure 4 SEM images of **a** reference, **b** MQ-modified CFs, as well as **c** plain CFs and **d** CFs modified with MQ after immersion in pore solution for 28 days.

(a) Ref   (b) MQ-CF

(c) Ref/28d   (d) MQ-CF/28d
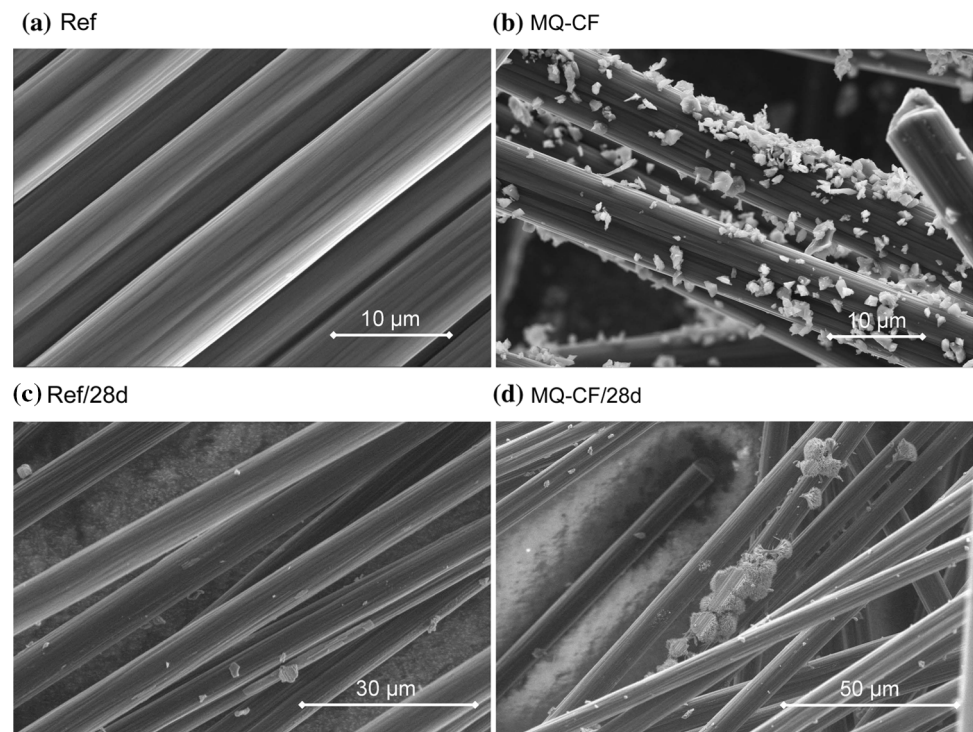
Figure 5 a ESEM image of the surface of MQ-modified CF (1 V, 15 min), and corresponding EDX mapping of **b** color composite for C, Si, and O elements; **c** Si in red; **d** O in blue.
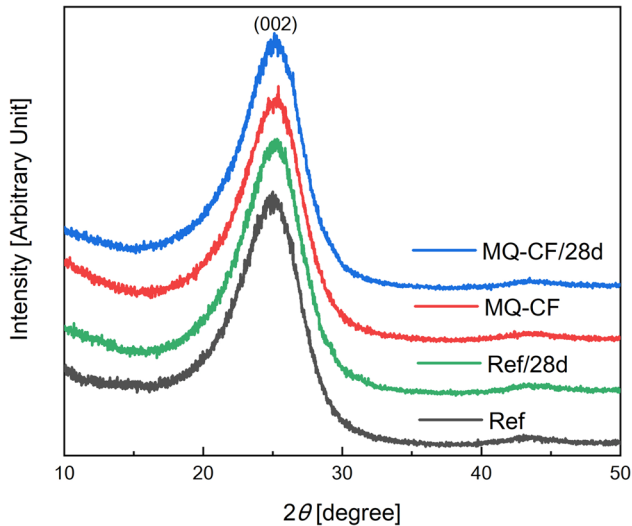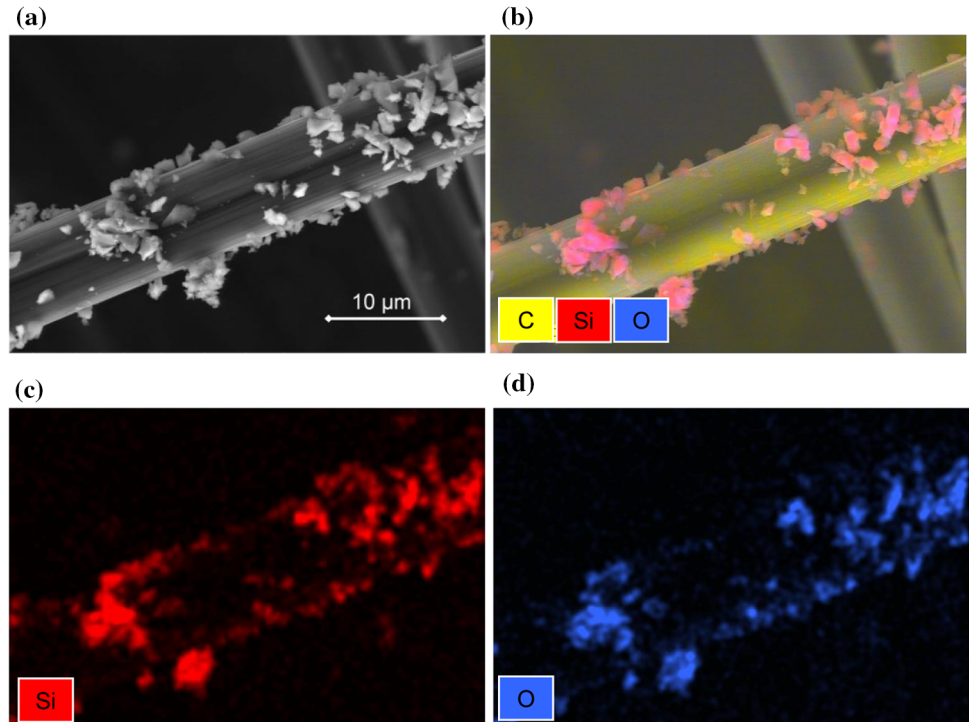
Figure 6 XRD spectra of untreated and electrophoretically modified CFs.

Table 4 Crystal size L_c and interlayer spacing d_{002} for untreated and EPD-modified CFs before and after immersion in cement pore solution for 28 days

Treatment	2θ [°]	d_{002} [nm]	β [rad]	L_c [nm]
Ref	25.00	0.36	0.0998	1.36
Ref/28d	25.14	0.35	0.0953	1.42
MQ-CF	25.20	0.35	0.0960	1.41
MQ-CF/28d	25.16	0.35	0.0939	1.44

The averaged graphite interlayer spacing d_{002} and the crystallite thickness L_c were derived by using Bragg and Debye–Scherrer equations as follows [44]:

$$n\lambda = 2d\sin\theta \tag{1}$$

$$L_c = \frac{K\lambda}{\beta\cos\theta} \tag{2}$$

where the wavelength of the X-rays λ is 0.15418 [44], θ represents half of the Bragg angle (2θ) in radians, d_{002} is the interlayer distance of graphite, β represents the full width at half-maximum (FWHM) in XRD profiles in radians [45], and $K = 0.9$ is the form factor for $L_{c(002)}$ [46].

The crystal characteristics of as-received CFs and modified samples are given in Table 4. For the original CFs, the largest interlayer distance (d_{002}=0.36 nm) and the smallest crystalline thickness (L_c=1.36 nm) were registered among all the samples. After 28-day immersion in cement pore solution, the d_{002} value slightly declined to 0.35 nm and the L_c value increased up to 1.42 nm.

The MQ-modified CFs before and after immersion in pore solution showed almost the same d_{002}-spacings of about 0.35 nm and thus also slightly lower than for the reference sample. It is worth noting that EPD modification afforded the larger crystalline dimension to the CFs, as indicated by higher L_c value of the MQ-CF sample (1.41 nm). This phenomenon of decrease in d_{002} value and increase in L_c value for the EPD-treated CFs has also been observed in a previous study [21]. After being immersed in pore solution, the MQ-coated CFs exhibited the largest crystalline size among all the samples (L_c=1.44 nm). An increase in crystalline dimension was also reported in [21, 47]. The decrease in d_{002} values after surface modification or immersion may be explained by improved layer plane stacking induced by removal of defects as discussed in the literature [48, 49].

These findings show that EPD treatment and the physicochemical environment of cementitious pore solution impact the microstructure of CFs resulting in altered physical and physicochemical properties of the material.

Raman spectroscopy

Raman spectroscopy was used to analyze the effect of EPD on the surface and structure of CFs. First-order Raman scattering of carbon allotropes, such as crystalline and amorphous graphite, graphene, carbon nanotubes, has been elaborately discussed in the literature [50–52], and the effect was exploited to derive insights into the system's molecular properties. Particularly, the resultant Raman bands between 1000^1 and $2000 \, \text{cm}^{-1}$, attributed to phonon/normal modes of the underlying carbon ring structure, are highly structure-sensitive. In this context, relevant features in the Raman spectrum are the so-called G and D peaks at around $1360 \, \text{cm}^{-1}$ and $1580 \, \text{cm}^{-1}$, respectively [53]. The G peak arises from single resonant scattering on E_{2g} phonons of the original carbon chain, while molecular origin of the D peak can be understood to represent the breathing mode of the carbon ring [50]. Thus, the latter is believed to be particularly sensitive to defects in the carbon system. In the context of exploring mechanical properties of CF [13, 53, 54] and other carbon allotropes [55], particularly the intensity ratio of D to G peak has been used as a measure for monitoring changes in the carbon structure.
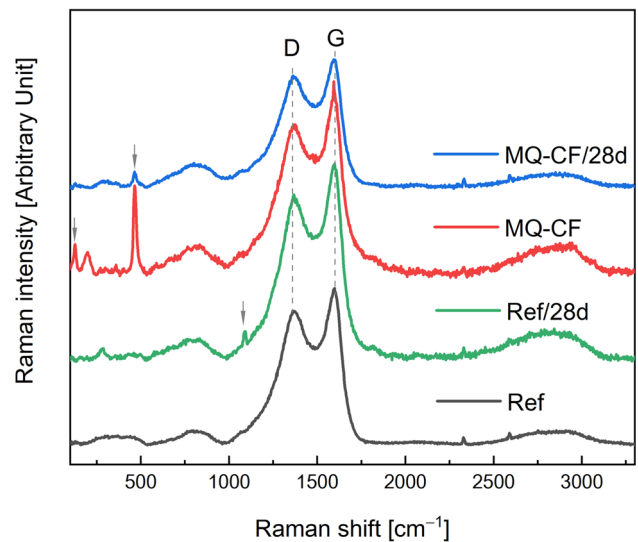

Figure 7 514-nm excited Raman spectra of untreated CF and MQ-modified CF before and after exposure to cement pore solution for 28 d.

Figure 7 shows the Raman spectra for untreated CF and modified CF before and after being immersed in cement pore solution. In the low-frequency region from 150 to $600 \, \text{cm}^{-1}$, differences depending on the treatment of the CF can be observed. In line with microscopy results shown above, successful decoration of CF with MQ particles via EPD could be verified by occurrence of MQ bands at $465 \, \text{cm}^{-1}$ and $151 \, \text{cm}^{-1}$.

The Raman spectrum of untreated CF immersed in pore solution is shown in Fig. 8. Weak carbonate signals could be noted at $1089 \, \text{cm}^{-1}$ (ν(C–O) modes) and $282 \, \text{cm}^{-1}$ (skeletal modes) [56]. After immersion in pore solution for 28d, fewer MQ particles were reflected by decreased intensity, which is in line with SEM results (Sect. Morphological analysis). However, no carbonate signals were found. Note, due to heterogeneous distribution of MQ on the CF surface, the lack of carbonate signals at the measured spots on the CF surface does not directly exclude the presence of $CaCO_3$ structures.

In the mid- and high-frequency region from 600 to $1600 \, \text{cm}^{-1}$, all spectra exhibited typical Raman features of graphite and are largely comparable to Raman data of CF yarns reported in other works [13, 53]. The envelope of bands from 1000 to $1700 \, \text{cm}^{-1}$ is dominated by the D band and the G band at about $1366 \, \text{cm}^{-1}$ and $1597 \, \text{cm}^{-1}$, respectively. For all measured samples, the positions of the G and D bands were found to be constant. In line
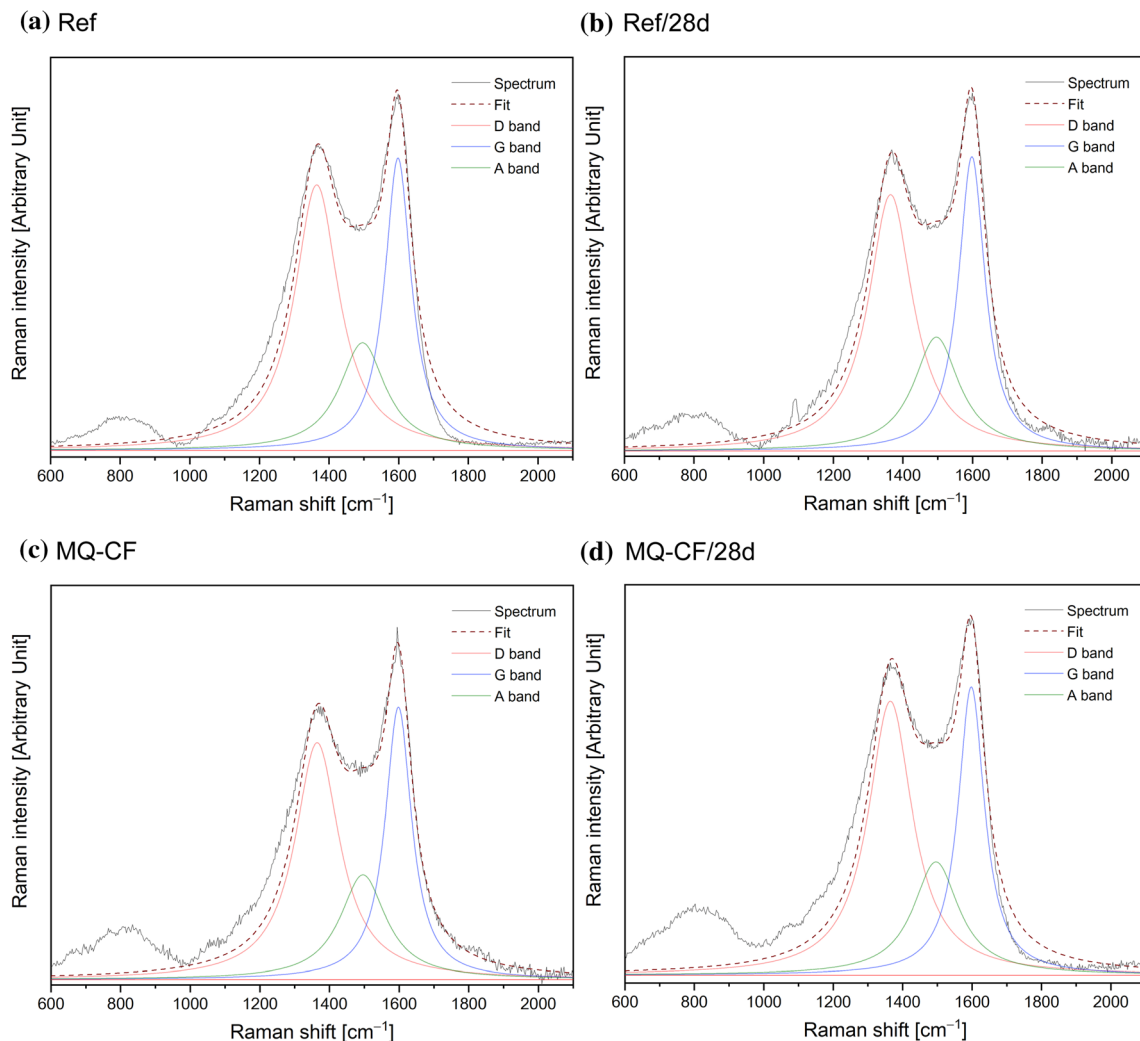
Figure 8 Raman spectra of untreated and MQ-modified CF with and without immersion in cement pore solution for 28d. The spectral region from 1000 to 1700 cm^{-1} was fitted with three Lorentzian bands representing the D (red), G (blue), and A (green) bands, respectively.

with other studies [50, 53], a broad background was noted from 1000 to 1600 cm^{-1} that is commonly attributed to the presence of amorphous carbon allotropes. To derive structural information, the carbon-specific spectral region from 1000 to 1600 cm^{-1} was fitted with three Lorentzian bands accounting for D, G, and an additional A band, respectively (Fig. 8). The A band (or D$_3$ band) at approximately 1490 cm^{-1} was introduced to account for spectral contribution from amorphous carbon allotropes, as proposed by other works [53, 57]. However, the molecular origin of the A band is controversial and is suspected to be correlated with surface modifications resulting from heteroatom binding and formation of functional groups on the graphite surface [53]. Figure 8 shows

the fitted curves satisfyingly reproducing the original spectra in the relevant frequency regions for all samples. Here, only the intensity of the fit bands was allowed to vary, while frequency and half-width were kept constant to keep the degree of freedom in the fit as lowest as possible.

Based on the fits, the peak areas derived from band fitting analysis (Fig. 8) were determined for D, G, and A bands. Table 5 shows the peak intensity ratios of the D band vs G band (I_D/I_G) as well as A band vs G band (I_A/I_G) for the relevant samples investigated in this study. It is commonly assumed that a high ratio of I_D/I_G can be considered to be lowered graphitic character of the sample [13, 53]. All modified samples show an increase of I_A/I_G to 0.66 and 0.68,

Table 5 Peak area ratios of D band to G band (I_D/I_G) and A band to G band (I_A/I_G)

Sample	I_D/I_G	I_A/I_G
Ref	1.52	0.64
Ref/28d	1.46	0.68
MQ-CF	1.46	0.66
MQ-CF/28d	1.59	0.68

Figure 9 TGA profiles of untreated CF (Ref) and the fibers modified with MQ before and after being stored in the cementitious pore solution for 28 days.

respectively, suggesting that both EPD treatment and exposure to cement pore solution induce microstructural change potentially resulting in amorphous carbon, considering that the I_D/I_G more differences can be observed. Both Ref/28d sample (tensile strength increased by 4%) and MQ-CF sample (tensile strength increased by 14%) exhibited lower I_D/I_G values than the reference, revealing less defects and more ordered sheath structure of CFs. Potentially mild etching effects occur, which decrease the number of strength-reducing flaws [21, 58]. MQ-CF/28d sample (tensile strength decreased by 20%) showed instead heightened I_D/I_G ratio, potentially due to ongoing oxidation and structural damage of the ordered CF layers, which is in line with the reduction of mechanical strength, cf. Sect. Tensile strength and modulus of untreated and electrophoretically modified CFs.

Thermogravimetric analysis

TGA measurements were taken to explore the thermal stability of untreated and EPD-treated CFs before and after being immersed in the cement pore solution for 28 days. The thermal degradation process of the samples occurred in the temperature range from approximately 600–850 °C, as depicted in Fig. 9.

For the CFs before exposure to pore solution, the significant oxidation process starts at around 650 °C. In more detail, 10% weight losses of the reference sample and the CFs coated with MQ were recorded at temperatures reaching 636 °C and 625 °C, respectively. Hence, the thermal stability of the modified fibers is slightly reduced due to the oxidation of CFs in electrochemical modification [59, 60].

After storing in cement pore solution, the oxidation of pristine CFs and MQ-modified fibers occurred at significantly lower temperatures. The 10% mass loss occurred for Ref/28d and MQ-CF/28d samples already at the temperature of 559 °C and 561 °C, respectively. Similar phenomena were observed in an earlier research by the authors [12], where the
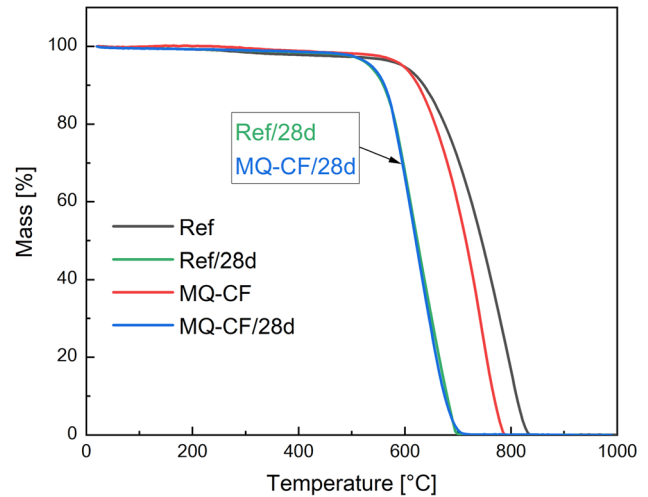
temperature stability of NS-modified CFs deteriorated after 14-day immersion in pore solution. This degradation could be induced by the oxidative damage of fiber itself in the high-alkaline environments of pore solution [61–63]. Meanwhile, as can be seen from the TGA profiles, the profiles of Ref/28d and MQ-CF/28d mainly overlay each other, which may denote that the thermostability of fibers is mainly influenced by the cementitious environment after being embedded in the matrices, while EPD treatment has only a minor impact.

Tensile strength and modulus of untreated and electrophoretically modified CFs

Figure 10 and Table 6 present the difference in tensile strength and modulus of elasticity for the CFs before and after electrophoretic treatment. The tensile strength of reference CFs increased by 4% after exposure to the cement pore solution, see Fig. 10a. This improvement might be related to the removal of fiber flaws, as discussed before in the RAMAN section. For the MQ-modified CFs, the tensile strength increased by 14% in comparison with untreated fibers. This indicates that the microstructural changes, as proven in the RAMAN part, induce also a change in the mechanical properties of the fibers. Moreover, according to Liu *et al.* [64], also oxidation processes occur during the electrochemical treatment yielding a reduction of sharp edges and micro-crack tips on the fiber surface. Thus, this surficial etching

Figure 10 **a** Tensile strength and **b** modulus of elasticity of untreated and EPD-treated CFs.
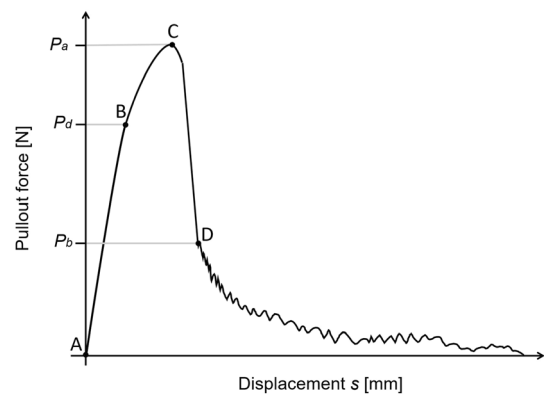

(a)

(b)
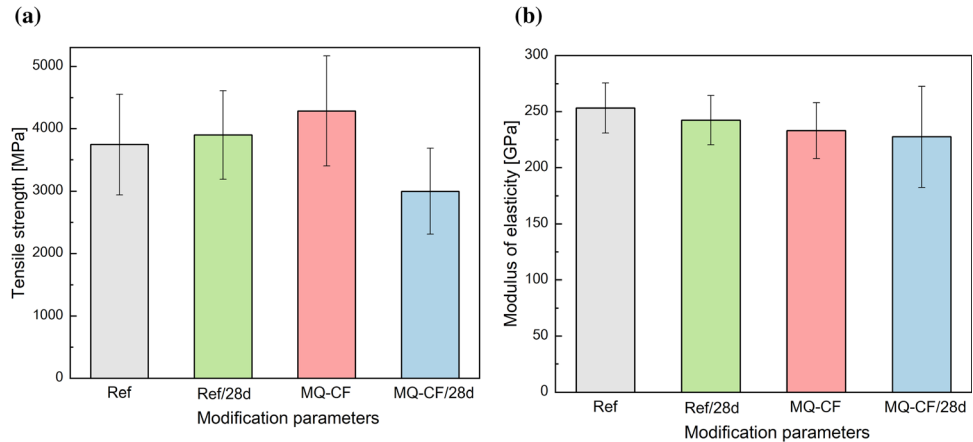
Table 6 Acquired tensile strengths and moduli of elasticity for reference and MQ-modified samples before and after exposure to cement pore solution for 28 days

Sample	Tensile strength [MPa]	Modulus of elasticity [GPa]
Ref	3746 ± 807	251 ± 28
Ref/28d	3901 ± 709	242 ± 22
MQ-CF	4283 ± 881	242 ± 16
MQ-CF/28d	2997 ± 688	228 ± 45

Figure 11 Representative force–displacement curve in single-fiber pullout tests.

effect of fiber flaws contributed to the augmentation in tensile strength as well. However, the MQ-CF/28d sample suffered a pronounced decrease in tensile strength, which can be traced back to the microstructural damage and the deterioration of severe flaws due to in-depth oxidation; cf. section Raman spectroscopy.

Figure 10b shows that exposure to pore solution and EPD treatment can negatively affect the modulus of elasticity of CFs. In comparison with the original fibers, its value decreased for Ref/28d, MQ-CF, and MQ-CF/28d samples by 3%, 3%, and 9%, respectively. Similar deterioration was also reported previously [12]. This minor descending tendency of the modulus after electrophoretic modification could be explained by the loss of carbon and fiber oxidation during the treatment process [65, 66]. Additionally, some microstructural changes after EPD treatment were observed, see sections. X-ray diffraction (XRD) and Raman spectroscopy. Thus, the decrease in modulus of elasticity could also result from the etching of the structurally ordered outer region of CF due to the oxidation process.

On a whole, EPD treatment was proved to have little effect on the tensile properties of CFs, while the

mechanical properties of CFs with EPD treatment could be more easily impaired owing to advanced oxidation.

## Pullout behavior of electrophoretically modified CFs

One-sided single-fiber pullout tests were used to obtain detailed information on interfacial properties between fiber and cementitious matrix. The typical idealized pullout curve with several characteristic points is shown in Fig. 11. The pullout process of a single-carbon filament toward the cement matrix mainly consists of four phases. In the first, elastic phase, the external force rises linearly from A to B, representing the linear-elastic stretching of the fiber at its free length. Subsequently, the debonding process beings at point B with a progressive interface fracture. After reaching the maximum peak load P_a at point C, a steep drop of force occurs which stops at

the maximal frictional force of P_b. In the last slippage phase, the interfacial interaction is mainly governed by friction and a slight slip-softening manner until complete pullout [41].

For estimating the mechanical anchorage effect of single CFs in the cement matrix, the apparent bond strength was calculated by dividing the maximum pullout force P_a by the interface area between fiber and matrix, as shown in Eq. (3) [41, 67].

$$\tau_{app} = \frac{P_a}{\pi d_f L_e} \tag{3}$$

where L_e is the fiber embedded length in a cement matrix and the d_f is the fiber's diameter.
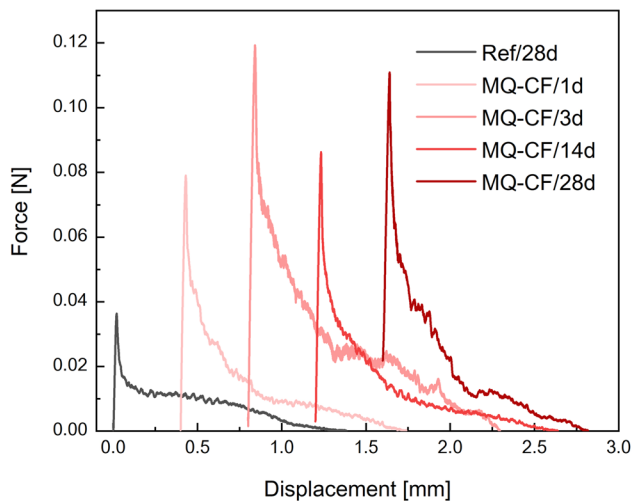

Figure 12 Representative pullout curves for untreated and treated CFs at various curing ages.

The onset of frictional slipping at point D was used to obtain the frictional resistance of the single filaments to the cement matrix, see Eq. (4) [41].

$$\tau_{fr} = \frac{P_b}{\pi d_f L_e} \tag{4}$$

The representative force–displacement curves of original and modified fibers after various hydration periods are presented in Fig. 12. Obviously, all modified samples showed a remarkable enhancement of bond performance in comparison with the original samples. With increasing age, the interfacial bond showed an ascending tendency for the MQ-modified samples. The pullout force-slip behavior for modified fiber and matrix at various curing ages will be quantitatively discussed in the following sections in terms of apparent and frictional bond strengths. Since bond performance between as-received CF (Ref) and cement was reported to be relatively poor for almost all curing ages [41], only pullout results for untreated samples at 28 days are presented in this study.

Figure 13a shows the apparent bond strengths (τ_{app}) for untreated and treated CFs at various curing ages. As can be seen, τ_{app} of MQ-CF/1d, MQ-CF/3d, MQ-CF/14d, and MQ-CF/28d was drastically enhanced by 95%, 173%, 115%, and 171%, respectively. The enhancement of bond performance is mainly attributable to an interfacial interlocking of the quartz particles during pullout, leading to an enhanced anchoring action. Additionally, the fine
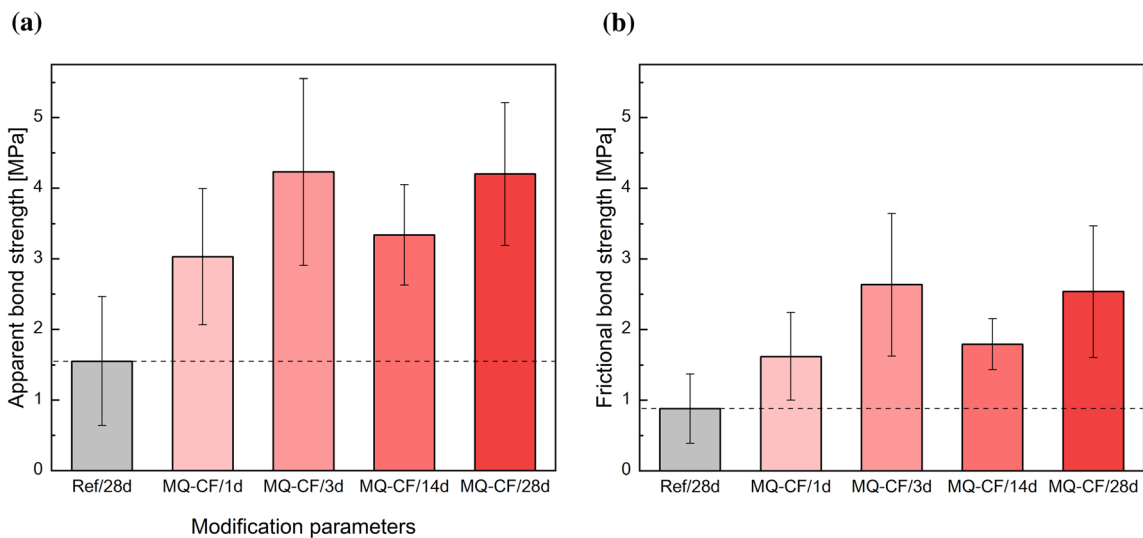
Figure 13 a Apparent bond strengths (τ_{app}) and **b** frictional bond strengths (τ_{fr}) of untreated and EPD-modified CFs.

quartz particles may accelerate the formation of C–S–H gel [32–34], in particular, at an early age [31, 35], due to the nucleation effect, thus densifying the fiber/cement matrix interphase.

Overall, the MQ-modified fiber showed an increase of τ_{app} value over time owing to the ongoing hydration. In particular, its pullout shear strength exhibited the highest value up to 4.2 MPa at 3 days, which can be ascribed to the rapid generation of cement hydrated products in the vicinity of fibers [41]. A similar phenomenon was reported in the previous research with NS [41].

Figure 13b presents the frictional bond strengths (τ_{fr}) for untreated and modified samples at varied curing times. The results show good agreement with the outcome for τ_{app}; cf. Fig. 13a. The relatively high value of τ_{fr} was registered for the MQ-modified samples cured for 3 days, too. The τ_{fr} value exhibited an augmentation by 84% for MQ-CF/1d, by 199% for MQ-CF/3d, by 104% for MQ-CF/14d, and by 188% for MQ-CF/28d, in comparison with that obtained for Ref/28d specimen. As aforementioned, the quartz coating could be capable of facilitating the hydration process at the fiber–cement interface, and therefore, provoking densification of the matrix at the peripheral zone of the fibers. Furthermore, the interlocking mechanism could be also enhanced, tailoring the frictional interaction at the fiber–cement interface.

Summary and conclusions

Electrophoretic deposition of MQ onto CF surfaces was performed to improve the bond behavior at the fiber–cement matrix interface and explore its effect on the microstructural and mechanical properties of CFs. MQ particles were successfully deposited on the fiber surfaces, as confirmed by microscopic observation. Electrochemical characterization and zeta-potential measurements indicated that the MQ colloids with a negative charge are relatively stable in aqueous suspension and that they can move toward CF electrode surfaces under applied voltage.

After EPD modification or exposure to cement pore solution, the modulus of elasticity and thermal stability of CFs were slightly impaired by oxidation during treatment, while the fiber strengths at room temperature showed an increase due to the removal of strength-reducing flaws by the etching effect and

the more structurally ordered graphitic crystallites of fiber surfaces. When the MQ-modified CFs were stored in the cement pore solution, the samples showed a decrease in graphite structures owing to advanced oxidation, therefore leading to a reduction in mechanical properties. Furthermore, it was also found that the storage in pore solution negatively affected the temperature stability of both original and modified fibers due to the strong alkalinity of the cementitious solution. Hence, future studies should focus on the long-term durability of EPD-modified CFs in cementitious composites.

Single-fiber pullout tests showed a drastic enhancement in pullout resistance of EPD-modified CFs embedded in the cementitious matrix. The apparent shear bond strength and frictional bond strength of CFs coated with MQ exhibited a pronounced increase after 28 days of curing. This is mainly attributed to an improved anchorage effect due to the coated MQ layers.

Based on these observations, it can be concluded that an EPD treatment of CF with micro-scaled quartz provides an effective way to improve the pullout behavior of CFs from cement matrices, especially for the frictional bonding. This eco-friendly, cost-efficient technology possesses also high controllability, making it suitable for industry-scale processing of long continuous CF rovings.

References

[1] Wang L, Chen L, Provis JL, Tsang DC, Poon CS (2020) Accelerated carbonation of reactive MgO and Portland cement blends under flowing CO2 gas. Cem Concr Compos 106:103489

[2] Li H, Liebscher M, Ranjbarian M, Hempel S, Tzounis L, Schröfl C, Mechtcherine V (2019) Electrochemical modification of carbon fiber yarns in cementitious pore solution for an enhanced interaction towards concrete matrices. Appl Surf Sci 487:52–58

[3] Du Y, Yang J, Thomas BS, Li L, Li H, Nazar S (2020) Hybrid graphene oxide/carbon nanotubes reinforced cement paste: an investigation on hybrid ratio. Constr Build Mater 261:119815

[4] Curosu I, Liebscher M, Burk S, Li H, Hempel S, Raak N, Rohm H, Mechtcherine V (2021) Influence of fiber type on the tensile behavior of high-strength strain-hardening cement-based composites (SHCC) at elevated temperatures. Mater Des 198:109397

[5] Curosu I, Liebscher M, Alsous G, Muja E, Li H, Drechsler A, Frenzel R, Synytska A, Mechtcherine V (2020) Tailoring the crack-bridging behavior of strain-hardening cement-based composites (SHCC) by chemical surface modification of poly (vinyl alcohol)(PVA) fibers. Cem Concr Compos 114:103722

[6] Mechtcherine V (2012) Towards a durability framework for structural elements and structures made of or strengthened with high-performance fibre-reinforced composites. Constr Build Mater 31:94–104

[7] Lu Z, Hanif A, Sun G, Liang R, Parthasarathy P, Li Z (2018) Highly dispersed graphene oxide electrodeposited carbon fiber reinforced cement-based materials with enhanced mechanical properties. Cem Concr Compos 87:220–228

[8] Li H, Liebscher M, Michel A, Quade A, Foest R, Mechtcherine V (2021) Oxygen plasma modification of carbon fiber rovings for enhanced interaction toward mineral-based impregnation materials and concrete matrices. Constr Build Mater 273:121950

[9] Donnini J, Corinaldesi V, Nanni A (2016) Mechanical properties of FRCM using carbon fabrics with different coating treatments. Compos B Eng 88:220–228

[10] de Andrade Silva F, Butler M, Hempel S, Toledo Filho RD, Mechtcherine V (2014) Effects of elevated temperatures on the interface properties of carbon textile-reinforced concrete. Cem Concr Compos 48:26–34

[11] Schneider K, Lieboldt M, Liebscher M, Fröhlich M, Hempel S, Butler M, Schröfl C, Mechtcherine V (2017) Mineral-based coating of plasma-treated carbon fibre rovings for carbon concrete composites with enhanced mechanical performance. Materials 10(4):360

[12] Li H, Liebscher M, Curosu I, Choudhury S, Hempel S, Davoodabadi M, Dinh TT, Yang J, Mechtcherine V (2020) Electrophoretic deposition of nano-silica onto carbon fiber surfaces for an improved bond strength with cementitious matrices. Cem Concr Compos 114:103777

[13] Lavagna L, Musso S, Ferro G, Pavese M (2018) Cement-based composites containing functionalized carbon fibers. Cem Concr Compos 88:165–171

[14] Corujeira Gallo S, Charitidis C, Dong H (2017) Surface functionalization of carbon fibers with active screen plasma. J Vac Sci Technol A Vac Surf Films 35(2):021404

[15] Li H, Liebscher M, Yang J, Davoodabadi M, Li L, Du Y, Yang B, Hempel S, Mechtcherine V (2022) Electrochemical oxidation of recycled carbon fibers for an improved interaction toward alkali-activated composites. J Clean Prod 368:133093

[16] Raphael N, Namratha K, Chandrashekar B, Sadasivuni KK, Ponnamma D, Smitha A, Krishnaveni S, Cheng C, Byrappa K (2018) Surface modification and grafting of carbon fibers: a route to better interface. Prog Cryst Growth Charact Mater 64:75–101

[17] An Q, Rider AN, Thostenson ET (2012) Electrophoretic deposition of carbon nanotubes onto carbon-fiber fabric for production of carbon/epoxy composites with improved mechanical properties. Carbon 50(11):4130–4143

[18] Park JK, Do I-H, Askeland P, Drzal LT (2008) Electrodeposition of exfoliated graphite nanoplatelets onto carbon fibers and properties of their epoxy composites. Compos Sci Technol 68(7–8):1734–1741

[19] Besra L, Liu M (2007) A review on fundamentals and applications of electrophoretic deposition (EPD). Prog Mater Sci 52(1):1–61

[20] Corni I, Ryan MP, Boccaccini AR (2008) Electrophoretic deposition: from traditional ceramics to nanotechnology. J Eur Ceram Soc 28(7):1353–1367

[21] Li H, Liebscher M, Micusik M, Yang J, Sun B, Yin B, Yu M, Mechtcherine V (2022) Role of pH value on electrophoretic deposition of nano-silica onto carbon fibers for a tailored bond behavior with cementitious matrices. Appl Surf Sci 600:154000

[22] Quercia G, Hüsken G, Brouwers H (2012) Water demand of amorphous nano silica and its impact on the workability of cement paste. Cem Concr Res 42(2):344–357

[23] Li L, Yang J, Li H, Du Y (2021) Insights into the microstructure evolution of slag, fly ash and condensed silica fume in blended cement paste. Constr Build Mater 309:125044

[24] Lin R-S, Wang X-Y, Zhang G-Y (2018) Effects of quartz powder on the microstructure and key properties of cement paste. Sustainability 10(10):3369

[25] Avet F, Snellings R, Diaz AA, Haha MB, Scrivener K (2016) Development of a new rapid, relevant and reliable (R3) test method to evaluate the pozzolanic reactivity of calcined kaolinitic clays. Cem Concr Res 85:1–11

[26] De Weerdt K, Haha MB, Le Saout G, Kjellsen KO, Justnes H, Lothenbach B (2011) Hydration mechanisms of ternary Portland cements containing limestone powder and fly ash. Cem Concr Res 41(3):279–291

[27] Suraneni P, Fu T, Azad VJ, Isgor OB, Weiss J (2018) Pozzolanicity of finely ground lightweight aggregates. Cem Concr Compos 88:115–120

[28] Suraneni P, Weiss J (2017) Examining the pozzolanicity of supplementary cementitious materials using isothermal calorimetry and thermogravimetric analysis. Cem Concr Compos 83:273–278

[29] Benezet J, Benhassaine A (1999) The influence of particle size on the pozzolanic reactivity of quartz powder. Powder Technol 103(1):26–29

[30] Benezet J, Benhassaine A (1999) Grinding and pozzolanic reactivity of quartz powders. Powder Technol 105(1–3):167–171

[31] Kadri E, Aggoun S, De Schutter G, Ezziane K (2010) Combined effect of chemical nature and fineness of mineral powders on Portland cement hydration. Mater Struct 43(5):665–673

[32] Garrault-Gauffinet S, Nonat A (1999) Experimental investigation of calcium silicate hydrate (CSH) nucleation. J Cryst Growth 200(3–4):565–574

[33] Gutteridge WA, Dalziel JA (1990) Filler cement: The effect of the secondary component on the hydration of Portland cement: part 2: fine hydraulic binders. Cem Concr Res 20(6):853–861

[34] Berodier E, Scrivener K (2014) Understanding the filler effect on the nucleation and growth of C-S-H. J Am Ceram Soc 97(12):3764–3773

[35] Bentz DP, Ferraris CF, Jones SZ, Lootens D, Zunino F (2017) Limestone and silica powder replacements for cement: early-age performance. Cem Concr Compos 78:43–56

[36] Donnini J, Basalo FDC, Corinaldesi V, Lancioni G, Nanni A (2017) Fabric-reinforced cementitious matrix behavior at high-temperature: experimental and numerical results. Compos Part B Eng 108:108–121

[37] Li H, Liebscher M, Zhao D, Yin B, Du Y, Yang J, Kaliske M, Mechtcherine V (2022) A review of carbon fiber surface modification methods for tailor-made bond behavior with cementitious matrices. Prog Mater Sci 132:101040

[38] Nolan R, Langer A, Harington J, Oster G, Selikoff I (1981) Quartz hemolysis as related to its surface functionalities. Environ Res 26(2):503–520

[39] Kosmulski M, Maczka E, Janusz W, Rosenholm JB (2002) Multiinstrument study of the electrophoretic mobility of quartz. J Colloid Interface Sci 250(1):99–103

[40] Ranjbarian M, Mechtcherine V (2018) A novel test setup for the characterization of bridging behaviour of single microfibres embedded in a mineral-based matrix. Cem Concr Comp 92:92–101

[41] Li H, Zhao D, Liebscher M, Yin B, Yang J, Kaliske M, Mechtcherine V (2022) An experimental and numerical study on the age depended bond-slip behavior between nano-silica modified carbon fibers and cementitious matrices. Cem Concr Compos 128:104416

[42] A Standard (1985) Zeta potential of colloids in water and waste water. ASTM Standard D, pp. 4187–82

[43] Park S-J, Seo M-K, Lee Y-S (2003) Surface characteristics of fluorine-modified PAN-based carbon fibers. Carbon 41(4):723–730

[44] Anderson DP (1991) Carbon fiber morphology. 2. Expanded wide-angle x-ray diffraction studies of carbon fibers. Dayton Univ Oh Research Inst

[45] Epp J (2016) X-ray diffraction (XRD) techniques for materials characterization. In: Materials characterization using nondestructive evaluation (NDE) methods. Elsevier, p 81–124. https://doi.org/10.1016/B978-0-08-100040-3.00004-3

[46] Jeffery JW (1971) Methods in X-ray crystallography.

[47] Li Z, Wang J, Tong Y, Xu L (2012) Anodic oxidation on structural evolution and tensile properties of

polyacrylonitrile based carbon fibers with different surface morphology. J Mater Sci Technol 28:1123–1129. https://doi.org/10.1016/S1005-0302(12)60181-9

[48] Adams P, Katzman H, Rellick G, Stupian G (1998) Characterization of high thermal conductivity carbon fibers and a self-reinforced graphite panel. Carbon 36(3):233–245

[49] Qiu L, Zheng X, Zhu J, Su G, Tang D (2013) The effect of grain size on the lattice thermal conductivity of an individual polyacrylonitrile-based carbon fiber. Carbon 51:265–273

[50] Ferrari AC, Meyer JC, Scardaci V, Casiraghi C, Lazzeri M, Mauri F, Piscanec S, Jiang D, Novoselov KS, Roth S (2006) Raman spectrum of graphene and graphene layers. Phys Rev Lett 97(18):187401

[51] Reich S, Thomsen C (2004) Raman spectroscopy of graphite. Philos Trans R Soc Lond A Math Phys Eng Sci 362:2271–2288

[52] Thapliyal V, Alabdulkarim ME, Whelan DR, Mainali B, Maxwell JL (2022) A concise review of the Raman spectra of carbon allotropes. Diam Relat Mater 127:109180

[53] Liu J, Tian Y, Chen Y, Liang J (2010) Interfacial and mechanical properties of carbon fibers modified by electrochemical oxidation in (NH4HCO3)/(NH4) 2C2O4· H2O aqueous compound solution. Appl Surf Sci 256(21):6199–6204

[54] Wu T, Lu C, Sun T, Li Y (2022) Study on Raman multi-peak fitting and structure quantitative analysis of PAN-based carbon fibers. J Mater Sci 57:15385–15412. https://doi.org/10.1007/s10853-022-07589-8

[55] Kinloch IA, Suhr J, Lou J, Young RJ, Ajayan PM (2018) Composites with carbon nanotubes and graphene: an outlook. Science 362(6414):547–553

[56] DeCarlo TM (2018) Characterizing coral skeleton mineralogy with Raman spectroscopy. Nat Commun 9(1):1–3

[57] Diaf H, Pereira A, Melinon P, Blanchard N, Bourquard F, Garrelie F, Donnet C (2022) Discrimination of different amorphous carbon by low fluence laser irradiation. Carbon Trends 9: 100195

[58] Bennett S, Johnson D, Johnson W (1983) Strength-structure relationships in PAN-based carbon fibres. J Mater Sci 18:3337–3347. https://doi.org/10.1007/BF00544159

[59] Besenhard J, Jakob J, Krebber U, Moeller P, Sauter R, Kurtze A, Kanani N, Meyer H, Hoerber J, Jannakoudakis A (1989) Anodische Oberflächen-und Volumenoxidation graphitischer Materialien in neutralen und alkalischen wäßrigen Lösungen/Anodic surface and bulk oxidation of graphitic materials in neutral and basic aqueous solutions. Zeitschrift für Naturforschung B 44(7):729–735

[60] Bismarck A, Pfeifer G, Springer J (2000) Study on surface- and mechanical fiber characteristics and their effect on epoxy composite properties tuned by continuous anodic carbon fiber oxidation. J Adhes Sci Technol 14(5):661–690

[61] Sugama T, Kukacka L, Carciello N, Galen B (1988) Oxidation of carbon fiber surfaces for improvement in fiber-cement interfacial bond at a hydrothermal temperature of 300 °C. Cem Concr Res 18(2):290–300

[62] Wang Y, Zhang S, Li G, Shi X (2019) Effects of alkali-treated recycled carbon fiber on the strength and free drying shrinkage of cementitious mortar. J Clean Prod 228:1187–1195

[63] Wang Y, Zhang S, Luo D, Shi X (2019) Effect of chemically modified recycled carbon fiber composite on the mechanical properties of cementitious mortar. Compos B Eng 173:106853

[64] Liu J, Tian Y, Chen Y, Liang J, Zhang L, Fong H (2010) A surface treatment technique of electrochemical oxidation to simultaneously improve the interfacial bonding strength and the tensile strength of PAN-based carbon fibers. Mater Chem Phys 122(2–3):548–555

[65] Bismarck A, Kumru M, Springer J, Simitzis J (1999) Surface properties of PAN-based carbon fibers tuned by anodic oxidation in different alkaline electrolyte systems. Appl Surf Sci 143(1):45–55

[66] Kozlowski C, Sherwood PM (1985) X-ray photoelectron-spectroscopic studies of carbon-fibre surfaces. Part 5.—The effect of pH on surface oxidation. J Chem Soc Faraday Trans 1 Phys Chem Condens Ph 81(11):2745–2756

[67] Rezaie AB, Liebscher M, Drechsler A, Synytska A, Mechtcherine V (2022) Tannic acid/ethanolamine modification of PE fiber surfaces for improved interactions with cementitious matrices. Cem Concr Compos 131:104573